Fluxons in high-impedance long Josephson junctions Ⓕ

Ⓘ Micha Wildermuth, Ⓘ Lukas Powalla, Ⓘ Jan Nicolas Voss, et al.

COLLECTIONS

Ⓕ   This paper was selected as Featured

View Online   Export Citation   CrossMark

ARTICLES YOU MAY BE INTERESTED IN

Enhancing ultrasound transmission and focusing through a stiff plate with inversely optimized auxiliary meta-lens
Applied Physics Letters **120**, 111701 (2022); https://doi.org/10.1063/5.0085462

Single-pulse all-optical partial switching in amorphous Dy_xCo_{1-x} and Tb_xCo_{1-x} with random anisotropy
Applied Physics Letters **120**, 112401 (2022); https://doi.org/10.1063/5.0077226

Temperature-dependent thermal resistance of phase change memory
Applied Physics Letters **120**, 113501 (2022); https://doi.org/10.1063/5.0081016

Fluxons in high-impedance long Josephson junctions ⒡

Micha Wildermuth,[1] ⒾⒹ Lukas Powalla,[1] ⒾⒹ Jan Nicolas Voss,[1] ⒾⒹ Yannick Schön,[1] ⒾⒹ Andre Schneider,[1] ⒾⒹ
Mikhail V. Fistul,[2,3] ⒾⒹ Hannes Rotzinger,[1,4,a)] and Alexey V. Ustinov[1,2,4,5] ⒾⒹ

AFFILIATIONS

[1]Physikalisches Institut, Karlsruhe Institute of Technology, 76131 Karlsruhe, Germany
[2]National University of Science and Technology MISIS, Moscow 119049, Russia
[3]Theoretische Physik III, Ruhr-Universität Bochum, 44801 Bochum, Germany
[4]Institute for Quantum Materials and Technologies, Karlsruhe Institute of Technology, 76131 Karlsruhe, Germany
[5]Russian Quantum Center, Skolkovo, Moscow 143025, Russia

[a)]Author to whom correspondence should be addressed: Rotzinger@kit.edu

ABSTRACT

The dynamics of fluxons in long Josephson junctions is a well-known example of soliton physics and allows for studying highly nonlinear relativistic electrodynamics on a microscopic scale. Such fluxons are supercurrent vortices that can be accelerated by bias current up to the Swihart velocity, which is the characteristic velocity of electromagnetic waves in the junction. We experimentally demonstrate slowing down relativistic fluxons in Josephson junctions whose bulk superconducting electrodes are replaced by thin films of a high kinetic inductance superconductor. Here, the amount of magnetic flux carried by each supercurrent vortex is significantly smaller than the magnetic flux quantum Φ_0. Our data show that the Swihart velocity is reduced by about one order of magnitude compared to conventional long Josephson junctions. At the same time, the characteristic impedance is increased by an order of magnitude, which makes these junctions suitable for a variety of applications in superconducting electronics.

The Josephson effect and weak links in superconductors[1,2] are at the basis of a wide range of applications within superconducting electronics and many related fields. The well-known examples are superconducting quantum interference devices,[3–6] voltage standard circuits,[7–9] and superconducting qubits.[10,11] The dynamics of charges and electromagnetic fields in Josephson junctions (JJs) is governed by the phase difference between the overlapping wave functions of superconducting electrodes.[1,2] In spatially extended JJs, the phase difference can vary in both time and space, which gives rise to a variety of propagating electromagnetic excitations. Common examples are linear waves formed by plasma oscillations of the Cooper pair density (Josephson plasmons), particle-like nonlinear wave packets with conserved amplitude, shape, and velocity (solitons),[12–16] and their bound states formed by soliton–antisoliton pairs oscillating around their common center of mass (breathers).[17,18]

In Josephson junctions, solitons occur in the form of Josephson vortices, often called fluxons,[13–15,19] which are pinned at the tunnel barrier plane and may propagate along this plane.[14,20,21] By applying a bias current across the junction, these vortices can be accelerated up to the speed of light inside the Josephson transmission line, which is noted as Swihart velocity $\bar{c}$.[22] The vortex's supercurrent is associated with a spatially localized 2π-kink in the superconducting phase difference across the junction. In "conventional" JJs, bulk electrodes provide complete magnetic screening, so that the fluxoid quantization of the phase in 2π units is linked to the magnetic flux carried by the vortex, which in turn is quantized in units of the magnetic flux quantum $\Phi_0 = h/2e$.[1,2]

The system's properties, such as velocity and spatial extension of a fluxon, are governed by the tunnel barrier's capacitance C and critical current density j_c as well as the lead inductance L_0 along the propagation direction. The precise controllability of these parameters qualifies Josephson vortices as excellent candidates for quantitative exploration of soliton physics. A preferred toy model is a quasi one-dimensional long Josephson junction (LJJ), whose length ℓ exceeds the characteristic spatial scale of the vortex λ_J, whereas the width w is much smaller than λ_J. Extensive

experiments in the past demonstrated, for instance, soliton–(anti)-soliton interactions,[19,23] interplay with cavity resonances,[24–28] Lorentz contraction of relativistic solitons,[21,29] and flux-flow dynamics of dense chains of solitons.[30,31] The latter regime finds its applications in microwave and millimeter-wave generation[32,33] and amplification of microwave signals.[34,35]

In all previous experiments with conventional JJs, the typical Swihart velocity was about a few percent of the light velocity in vacuum, while the junction's characteristic impedance was typically less than a few ohms.[36–38] These parameters are limited by the electrode's geometric inductance, which is given by the magnetic field penetration depth in the bulk superconducting electrodes and confined by the feasible structure size. In particular, the very low characteristic impedance of LJJs remained the major obstacle limiting their applications in superconducting electronics.

In this work, we overcome the above constraints by at least one order of magnitude via replacing the bulk electrodes of LJJ with a high kinetic inductance superconductor (HKIS), which increases the total inductance of the Josephson transmission line beyond the purely geometrical limit. Using the sine-Gordon model, we evaluate the impact of kinetic inductance on the Swihart velocity, Josephson length, and junction impedance. We verify these predictions by transport measurements at different magnetic fields, temperatures, and under microwave irradiation. We demonstrate a reduction of the Swihart velocity by one order of magnitude compared to the conventional junctions. Correspondingly, we estimate the characteristic impedance of our junctions to be a few tens of ohms, opening the way toward matching them to standard 50-ohm microwave cables and circuits.

Conventional LJJs can theoretically be modeled by lumped elements of resistively and capacitively shunted junctions[1,39,40] in the z-direction, which are extended along the x-axis and, thus, connected via inductive leads. The resulting perturbed sine-Gordon equation[12,19]

$$\partial_{\tau\tau}\varphi - \partial_{\chi\chi}\varphi + \sin\varphi = \gamma - \alpha\partial_\tau\varphi \qquad (1)$$

describes the junction's phase dynamics $\varphi(\chi, \tau)$. The time t and the spatial coordinate x are normalized to $\tau = \omega_{\mathrm{p}}t$ and $\chi = x/\lambda_{\mathrm{J}}$, respectively, with the Josephson plasma frequency $\omega_{\mathrm{p}} = (2\pi j_c/c\Phi_0)^{1/2}$ as inverse timescale and the Josephson penetration length $\lambda_{\mathrm{J}} = (\Phi_0/2\pi j_c L_0^\square)^{1/2}$ as the characteristic length. Here, j_c denotes the critical current density of the tunnel barrier, $c = C/lw$ its specific capacitance, and $L_0^\square$ the lead inductance per square. The left side of the perturbed sine-Gordon equation (1) is a wave equation, which describes the Josephson transmission line with the characteristic (Swihart) velocity $\bar{c} = \lambda_{\mathrm{J}}\omega_{\mathrm{p}} = (cL_0^\square)^{-1/2}$.[22] The terms on the right side of Eq. (1) denote perturbations, namely, a normalized bias current density $\gamma = j_b/j_c$, and Ohmic dissipation due to quasiparticle tunneling α.

The sine-Gordon model remains valid[41] even with additional lumped elements of kinetic inductance L_k in the electrodes. Here, we complement $L_0^\square$ with a kinetic part. This additional kinetic inductance of the electrode material comes along with a larger magnetic field penetration depth λ_{L}, which significantly modifies the vortex shape in such LJJs [see Figs. 1(c) and 1(d)]. The vortex current distributes inhomogeneously over the whole film thicknesses of the HKIS electrodes d_1, d_2. This yields reduced effective participation of the bulk kinetic inductance to the Josephson length λ_{J}. We take this effect into account
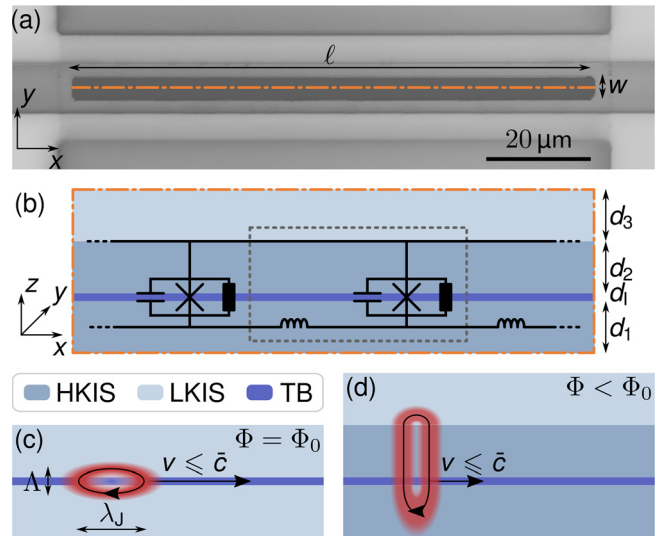

FIG. 1. (a) Micrograph of a long junction (dark gray area) in quasi-overlap geometry in the top view and (b) schematic cross section of the junction stack (along the dash-dotted line). The junction consists of layers of a high kinetic inductance superconductor (HKIS), an insulating tunnel barrier (TB), and a HKIS proximitized by low kinetic inductance superconductor (LKIS). The equivalent circuit of the LJJ's unit cell (dashed gray line) consists of a resistively and capacitively shunted junction across the TB together with inductive leads. (c) Josephson vortices (schematically shown as reddish ring current) arise in conventional Josephson junction with bulk LKISs as fluxons, each of them carrying one magnetic flux quantum Φ_0. (d) In impedance-tailored junctions including HKISs, Josephson vortices appear as fluxoids, which have reduced length, speed, and magnetic flux.

by introducing a geometrical factor $0 < g(\vec{r}) < 1$, such that for the junction's total lead inductance holds $L_0^\square = L_g^\square + g(\vec{r})L_k^\square$.

Compared to conventional long Josephson junctions, here the enlarged $L_0^\square$ results in slower Swihart velocity $\bar{c} \sim (L_0^\square)^{-1/2}$ and smaller vortex size $\lambda_{\mathrm{J}} \sim (L_0^\square)^{-1/2}$[41] while the junction impedance $Z = (L_0^\square/c)^{1/2}/w$,[42] correspondingly, increases. The lead inductance $L_0^\square$ along z [see Fig. 1(b)] plays a minor role for supercurrent oscillations across the barrier that is why the change in $L_0^\square$ does not affect the Josephson plasma frequency, to the first order. Furthermore, a substantial fraction of the vortex's total 2π phase winding drops at the dominating kinetic inductance, which generates no magnetic field and results in incomplete magnetic screening. The phase winding (fluxoid) quantization remains valid, but it does no longer necessitate quantized magnetic flux. The magnetic flux transported by a Josephson vortex Φ is, thus, significantly smaller than Φ_0, so that this kind of vortex can be more correctly noted as "fluxoid" instead of "fluxon." Similar fluxoids were previously observed in arrays of JJs,[43] where the current distribution is predefined by the array geometry. Our approach to impedance-tailored LJJs provides fluxoids in a continuous Josephson medium where the current distribution evolves with no spatial constraints.

The high kinetic inductance superconductor of our choice is a thin film of granular aluminum oxide (AlO$_x$), which have been used to establish macroscopic circuit quantum electrodynamics. This material consists of pure aluminum grains separated by intrinsic nanoscale tunnel barriers (TB),[45] which strongly influence both the normal and the superconducting transport properties ($T_c = 1.6$–2.0 K). In the

TABLE I. Properties of the fabricated trilayers. The normal conducting sheet resistance of the bottom electrode $R_n^\square$ is extracted from the film deposition. The critical current densities j_c are determined from squared junctions, and Ambegaokar–Baratoff estimations coincide to switching current measurements with junction areas of $(20\,\mu m)^2$. Magnetic thickness Λ^{exp} and Josephson penetration depth λ_J are derived from the critical current's magnetic field dependence of inline junctions at $T \approx 300$ mK, from which also the geometry factor $g(\vec{r})$ follows. From overlap junctions, the Swihart velocity $\bar{c}$ and the impedance Z is acquired from the periodicity of zero-field and Fiske steps at around 1 K.

Trilayer	$R_n^\square$ (Ω)	j_c (A cm^{-2})	Λ^{exp} (nm)	λ_J (μm)	$g(\vec{r})$ (10^{-2})	$\bar{c}_{zfs}/c_0$ (10^{-3})	$\bar{c}_{FS}/c_0$ (10^{-3})	Z (Ω)
A	38	0.32 ± 0.03	69 ± 2	LJJ limit not reached for $\ell \leq 120\,\mu$m			6.56 ± 0.03	2.79 ± 0.04
B	75	12.5 ± 0.3	72 ± 9	17.2 ± 2.2	15 ± 4	4.27 ± 0.06	3.64 ± 0.02	4.11 ± 0.06
C	778	1.90 ± 0.01	94 ± 9	19.5 ± 1.8	13 ± 3	3.37 ± 0.08	3.22 ± 0.03	14.0 ± 0.4

superconducting state, this granular material can be considered as a disordered network of Josephson junctions,[45] each of them providing a kinetic-type Josephson inductance[1] related to the junction normal state tunnel resistance R_n and the superconducting gap Δ by $L_k = \hbar R_n/\pi\Delta$.[46–50] The conductivity and inductance of HKIS formed by AlO$_x$ can vary over five orders of magnitude,[51,52] depending on the oxygen concentration in the nanoscale TBs,[53] which is controlled by the oxygen partial pressure during the reactive sputtering process.[49] This enormous versatility enables us using AlO$_x$ for different purposes, e.g., for depositing junctions with an HKIS in the bottom electrode, for depositing an insulating TB, and for forming a top electrode as a combination of HKIS and pure aluminum, as illustrated in Fig. 1(b). As summarized in Table I, we have fabricated three different junction stacks (A, B, and C) with varied values of $L_k^\square$ and j_c.

Since the normal sheet resistance $R_n^\square$ is the crucial parameter to obtain the desired kinetic inductance per unit square $L_k^\square$, we monitor both the film thickness d and sheet resistance $R_n^\square$ during the film deposition. This *in situ* $R(d)$ measurement allows us to fit the theoretical model for fine-grained polycrystalline thin films by Mayadas *et al.*[44] and to determine the specific resistance ρ_0. For sample A, its value is $\rho_0 = 70.7 \pm 0.2\,\mu\Omega$ cm yielding $R_n^\square \approx 35\,\Omega$ for a 20 nm thick film (for details, see the supplementary material, S1).

As the oxygen partial pressure can be adjusted during sputtering process, this kind of measurement is a powerful tool to achieve the aimed kinetic inductance value, with an accuracy of about 10 %, at a fixed film thickness. Figure 2 depicts such adjustments as knees and the creation of a tunnel barrier (emphasized in the inset). By reaching the targeted resistance at the end of the static oxidation process, we can assume the complete oxidation of the aluminum layer and also estimate the barrier thickness.

The junctions were patterned from trilayers by using etching and anodic oxidization processes.[54,55] The fabricated JJs were intentionally varied in length (20–120 μm), width (2–5 μm), and geometry. The latter defines the distribution of the bias current over the junction[56,57] and, therefore, affects the vortex dynamics. As discussed in detail in the supplementary material, S1, we fabricated junctions of square, inline, and (quasi-) overlap geometries.[58] We characterized the fabricated JJs [see Fig. 1(a)] by transport measurements at millikelvin temperatures and determined their characteristic parameters λ_J, $\bar{c}$, and ω_p independently.

In the first experiment, we determine the fluxoid's spatial extensions in both x and z directions, the Josephson length λ_J, and the magnetic thickness Λ of the tunnel barrier from measurements of the dependence of the critical current on magnetic field applied in the plane of the tunnel barrier. Examples of such critical current vs field patterns are depicted in Fig. 3. In high in-plane magnetic fields, where

the junction is considered to be completely penetrated by magnetic flux along the x axis, Λ is determined from the critical current's periodicity ΔB_a by $\Lambda = \Phi_0/\ell\Delta B_a$. As can be seen in Table I, L_k affects Λ, since the proximitized top electrode's London penetration depth λ_L enlarges with increasing L_k, whereas the bottom electrode of each stack is in the thin film limit $d_1 \ll \lambda_{L1}$ and, thus, contributes to Λ with $d_1/2$.[61] Together with the first critical field H_{c1}, above which vortices can enter the junction, we calculate the vortex size $\lambda_J = \Phi_0/\pi\mu_0 H_{c1}\Lambda$[62] and the kinetic inductance contributing locally to λ_J. The comparison of this value $g(\vec{r})L_k^\square$ with the kinetic inductance of the bottom layer $L_k^\square$, estimated from the resistance $R_n^\square$ measured *in situ* as $R(d)$ during the sample deposition, yields the geometry factor $g(\vec{r})$ on the order of 10^{-1}, as given in Table I.

In a second experiment, we determine the Swihart velocity from equidistant subgap current singularities originating in junction cavity mode excitations. In zero magnetic fields, these excitations are Josephson vortices, which are accelerated by the bias current, causing a Lorentz force, and reflected at the edges while reversing their polarity. Such resonant vortex oscillations manifest as current steps at integer multiples of the first zero-field step (ZFS) $V_1^{ZFS} = \Phi_0\bar{c}/\ell$.[25] Another kind of current singularities arises above the critical magnetic field where the Josephson frequency of a biased junction excites electromagnetic standing waves in the junction cavity. Such singularities are known as Fiske steps (FS) and occur at voltages with half the
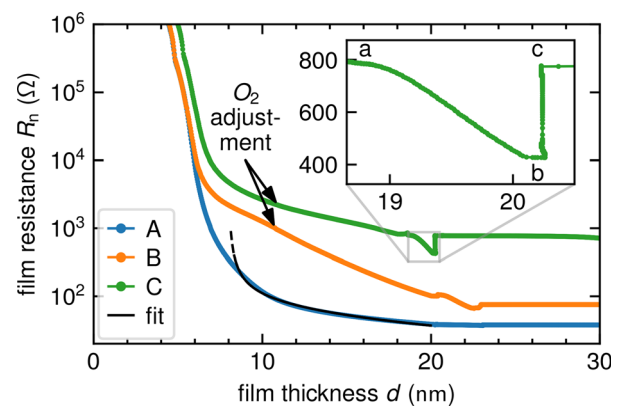
FIG. 2. *In situ* resistance monitoring during different trilayer depositions. The fit of the thickness dependent normal resistance $R_n(d)$ to the model of fine-grained polycrystalline thin films by Mayadas *et al.*[44] allows us to estimate the final resistance and to readjust the oxygen partial pressure if needed (trilayers B and C). The inset points out the tunnel barrier creation by deposition of pure Al (a) and (b) and subsequent static oxidation (b) and (c).

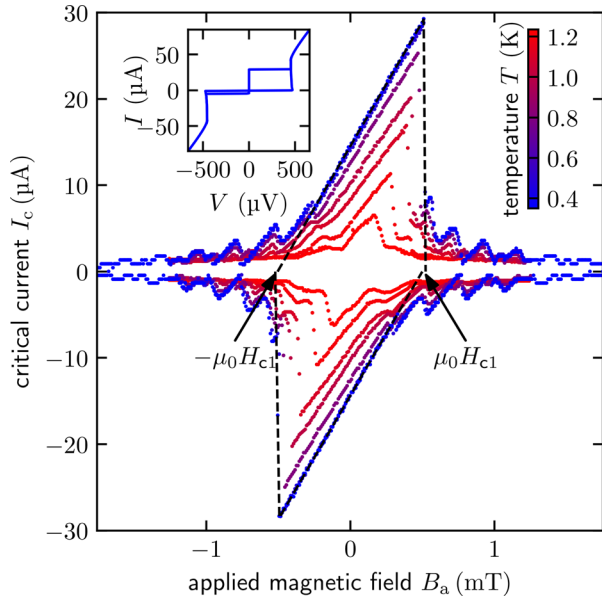**FIG. 3.** Magnetic diffraction pattern of a $110 \times 5\,\mu m^2$ long junction of trilayer B in inline geometry at different temperatures. The linear decrease in the Meissner phase confirms the long junction limit, and the extrapolated root of the mainlobe corresponds to $\pm H_{c1}$. The asymmetric lobes arise because of inhomogeneously distributed bias currents and different electrode inductances.[57,59,60] The inset shows an IV-characteristic at the main maxima with large hysteresis implying high quality factors.

FIG. 4. Current singularities of $100 \times 5\,\mu m^2$ and $110 \times 5\,\mu m^2$ long junctions of sample B in quasi-overlap geometry without and with magnetic fields, respectively. The dark gray line and the gray shaded area display the fits to Eq. (2) and their errors. (a) Zero-field steps arise only with sufficient damping in the junctions, which is realized by temperatures just below the critical temperature $T_c \approx 1.25\,K$. (b) Fiske steps occur at different magnetic fields and their characteristic rounded shape originates from the increased damping at $T = 1.0\,K$.

periodicity of ZFS $V_1^{FS} = \Phi_0 \bar{c}/2l$.[26–28] As the vortex propagation velocity depends on the bias current γ and the damping parameter α, the characteristic shape of the nth ZFS step is given by[15]

$$V_n^{ZFS}(\gamma) = V_1^{ZFS} \frac{n}{\sqrt{1 + \left(\frac{4\alpha}{\pi\gamma}\right)^2}}. \qquad (2)$$

The Swihart velocity $\bar{c}$ is determined by the periodicity of the current singularities and the known junction length ℓ (see Table I). As the junctions are underdamped (note the large hysteresis between critical and retrapping currents in the IV characteristics in the inset of Fig. 3), for reliably observing these current singularities arising from the sub-gap resistance branch, it helps to increase the damping by increasing temperature of the sample. Then, however, the Stewart–McCumber branch cuts the lower part of the higher-order steps, as shown in Fig. 4. For underdamped junctions, cavity oscillations are unstable for $\omega \lesssim \omega_p$,[63,64] which explains missing the first FS in Fig. 4.

In the third experiment, we determine the Josephson plasma frequency ω_p by measuring the plasma resonance of a square-shaped junction made of the trilayer B. The Josephson plasma oscillations are excited by applying external microwave irradiation. Resonant, subharmonic, or superharmonic driving[65] causes a multi-valued switching current from the zero to the nonzero voltage state. The secondary peaks in the switching current distribution[65–67] (see inset of Fig. S3 in the supplementary material, S2.2) are identified as resonant currents, for which the fixed external drive frequency equals the Josephson plasma resonance frequency ω_0, its integer multiples, or its fractions
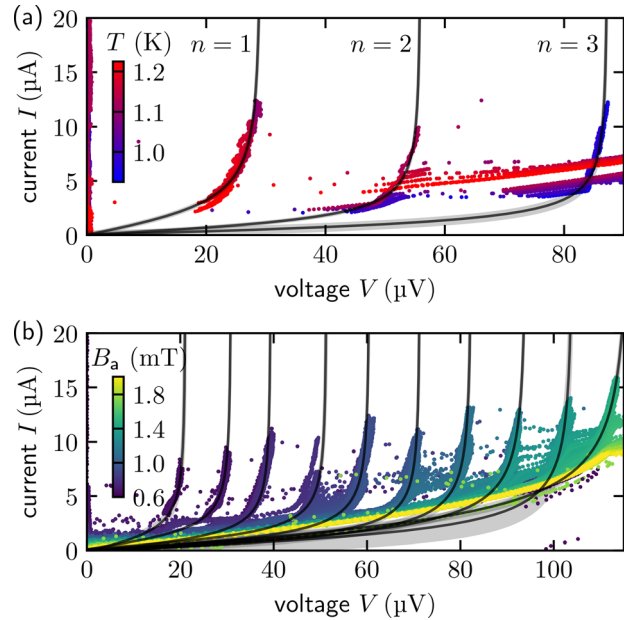
of ω_0. Since the bias current tilts the washboard potential of a JJ[68] and, thus, affects its shape, the associated internal oscillation frequency holds $\omega_0(\gamma) = \omega_p(1 - \gamma^2)^{1/4}$.[69] Orthogonal distance regression, as shown in Fig. S3, yields the plasma frequency $\omega_p/2\pi = 13.28 \pm 0.05\,GHz$, the critical current $I_c = 8.36 \pm 0.08\,\mu A$, and, hence, the specific tunnel barrier capacitance $c = 36.4 \pm 0.04\,fF\,\mu m^{-2}$.

To analyze the impact of the electrode's kinetic inductance on LJJs, their characteristic parameters, listed in Table I, are compared with estimations for conventional LJJs with equal tunnel barrier properties j_c and c, but made from pure aluminum. Here, we assume that pure aluminum electrodes have negligible kinetic inductance. The result of this comparison is that the electrode's kinetic inductance reduces both the Josephson length λ_J and the Swihart velocity $\bar{c}$ by a factor of up to 40, while the Josephson plasma frequency ω_p remains nearly unchanged. Accordingly, the wave impedance of LJJs is increased by the same factor. The inductance contributing to Josephson plasma oscillations is dominated by the macroscopic stack TB rather than the nanoscopic TBs in AlO$_x$ due to the much stronger intergrain coupling so that the increase in L_k can be neglected to the first order. The combination of the independently measured parameters corresponds to the conventional sine-Gordon model with modified $\bar{c} = \lambda_J \omega_p$.

In conclusion, our results demonstrate a significantly reduced Swihart velocity in long Josephson junctions fabricated with high kinetic inductance electrodes. In our work, we used disordered oxidized aluminum as a high kinetic inductance superconductor. Our experiments demonstrate a decrease in the vortex's size and a

reduction of its limiting (Swihart) velocity by about one order of magnitude in comparison with conventional LJJs. The measured Swihart velocities down to a small fraction of 3×10^{-3} of the light velocity in vacuum, in turn, correspond to an increase junction's wave impedance up to $14\,\Omega$ compared to $4\,\Omega$ of conventional, similarly made LJJs. The high-kinetic inductance electrodes, thus, enable tailoring the junction impedance and facilitate solving the long-standing problem of impedance matching LJJs to external circuits and $50\,\Omega$ cables. Matching the impedance to external loads is crucial for increasing the efficiency of Josephson flux-flow oscillators used for microwave generation and amplification. Furthermore, the reduction of vortex size results in fewer charges participating in internal junction dynamics, a smaller effective capacitance over the vortex area C_{eff}, and thus, increases the effective charging energy $E_{\text{c,eff}} = q^2/2C_{\text{eff}}$. As $E_{\text{c,eff}}$ plays the key role in experimentally reaching the quantum regime of Josephson vortex dynamics,[70] high kinetic inductance electrodes also facilitate observing the quantum electrodynamics phenomena in long Josephson junctions.

See the supplementary material for more information about the experimental details, junction characterization, and plasma frequency measurements.

AUTHOR DECLARATIONS
Conflict of Interest

The authors have no conflicts to disclose.

DATA AVAILABILITY

The data that support the findings of this study are available from the corresponding author upon reasonable request.

REFERENCES

[1]B. D. Josephson, Rev. Mod. Phys. **36**, 216 (1964).
[2]B. D. Josephson, Adv. Phys. **14**, 419 (1965).
[3]R. C. Jaklevic, J. Lambe, A. H. Silver, and J. E. Mercereau, Phys. Rev. Lett. **12**, 159 (1964).
[4]J. E. Zimmerman, P. Thiene, and J. T. Harding, J. Appl. Phys. **41**, 1572 (1970).
[5]J. Mercereau, Rev. Phys. Appl. **5**, 13 (1970).
[6]J. Clarke, Philos. Mag. **13**, 115 (1966).
[7]B. N. Taylor, W. H. Parker, D. N. Langenberg, and A. Denenstein, Metrologia **3**, 89 (1967).
[8]B. F. Field, T. F. Finnegan, and J. Toots, Metrologia **9**, 155 (1973).
[9]C. A. Hamilton, Rev. Sci. Instrum. **71**, 3611 (2000).
[10]Y. Makhlin, G. Schön, and A. Shnirman, Nature **398**, 305 (1999).
[11]J. Clarke and F. K. Wilhelm, Nature **453**, 1031 (2008).
[12]A. Barone, F. Esposito, C. Magee, and A. Scott, La Rivista del Nuovo Cimento **1**, 227 (1971).
[13]A. C. Scott, F. Y. F. Chu, and D. W. McLaughlin, Proc. IEEE **61**, 1443 (1973).
[14]A. C. Scott, F. Y. F. Chu, and S. A. Reible, J. Appl. Phys. **47**, 3272 (1976).
[15]D. W. McLaughlin and A. C. Scott, Phys. Rev. A **18**, 1652 (1978).
[16]P. Lomdahl, J. Stat. Phys. **39**, 551 (1985).
[17]D. J. Kaup and A. C. Newell, Proc. R. Soc. London, Ser. A **361**, 413 (1978).
[18]Y. S. Kivshar and B. A. Malomed, Rev. Mod. Phys. **61**, 763 (1989).
[19]A. V. Ustinov, Phys. D **123**, 315 (1998).
[20]I. Kulik, JETP **24**, 1307 (1967); available at https://ui.adsabs.harvard.edu/abs/1967JETP...24.1307K/abstract.
[21]A. Matsuda and T. Kawakami, Phys. Rev. Lett. **51**, 694 (1983).
[22]J. C. Swihart, J. Appl. Phys. **32**, 461 (1961).
[23]A. Fujimaki, K. Nakajima, and Y. Sawada, Phys. Rev. Lett. **59**, 2895 (1987).
[24]J. T. Chen, T. F. Finnegan, and D. N. Langenberg, Physica **55**, 413 (1971).
[25]T. Fulton and R. Dynes, Solid State Commun. **12**, 57 (1973).
[26]M. D. Fiske, Rev. Mod. Phys. **36**, 221 (1964).
[27]I. O. Kulik, ZhPmR **2**, 134 (1965); available at https://ui.adsabs.harvard.edu/abs/1965ZhPmR...2..134K/abstract.
[28]I. O. Kulik, Sov. Phys.-Tech. Phys. **12**, 111 (1967).
[29]A. Laub, T. Doderer, S. G. Lachenmann, R. P. Huebener, and V. A. Oboznov, Phys. Rev. Lett. **75**, 1372 (1995).
[30]K. Yoshida, F. Irie, and K. Hamasaki, J. Appl. Phys. **49**, 4468 (1978).
[31]K. Nakajima, H. Ichimura, and Y. Onodera, J. Appl. Phys. **49**, 4881 (1978).
[32]T. Nagatsuma, K. Enpuku, F. Irie, and K. Yoshida, J. Appl. Phys. **54**, 3302 (1983).
[33]V. P. Koshelets, P. N. Dmitriev, A. B. Ermakov, A. S. Sobolev, A. M. Baryshev, P. R. Wesselius, and J. Mygind, Supercond. Sci. Technol. **14**, 1040 (2001).
[34]T. Nagatsuma, K. Enpuku, H. Iwakura, and K. Yoshida, Jpn. J. Appl. Phys. **24**, L599 (1985).
[35]J. E. Nordman, Supercond. Sci. Technol. **8**, 681 (1995).
[36]A. Barone and G. Paterno, *Physics and Applications of the Josephson Effect* (Wiley, New York, 1982).
[37]K. K. Likharev, *Dynamics of Josephson Junctions and Circuits* (Gordon and Breach Science Publishers, Philadelphia, PA, 1986).
[38]E. Holdengreber, E. Schacham, and E. Farber, in Antennas and Propagation Conference 2019 (APC-2019), 2019; available at https://ieeexplore.ieee.org/abstract/document/9112858.
[39]W. C. Stewart, Appl. Phys. Lett. **12**, 277 (1968).
[40]D. E. McCumber, J. Appl. Phys. **39**, 3113 (1968).
[41]G. L. Alfimov and A. F. Popkov, Phys. Rev. B **52**, 4503 (1995).
[42]D. N. Langenberg, D. J. Scalapino, and B. N. Taylor, Proc. IEEE **54**, 560 (1966).
[43]H. S. J. van der Zant, F. C. Fritschy, T. P. Orlando, and J. E. Mooij, Phys. Rev. Lett. **66**, 2531 (1991).
[44]A. F. Mayadas, M. Shatzkes, and J. F. Janak, Appl. Phys. Lett. **14**, 345 (1969).
[45]G. Deutscher, H. Fenichel, M. Gershenson, E. Grünbaum, and Z. Ovadyahu, J. Low Temp. Phys. **10**, 231 (1973).
[46]D. C. Mattis and J. Bardeen, Phys. Rev. **111**, 412 (1958).
[47]R. E. Glover and M. Tinkham, Phys. Rev. **108**, 243 (1957).
[48]A. J. Annunziata, D. F. Santavicca, L. Frunzio, G. Catelani, M. J. Rooks, A. Frydman, and D. E. Prober, Nanotechnology **21**, 445202 (2010).
[49]H. Rotzinger, S. T. Skacel, M. Pfirrmann, J. N. Voss, J. Münzberg, S. Probst, P. Bushev, M. P. Weides, A. V. Ustinov, and J. E. Mooij, Supercond. Sci. Technol. **30**, 025002 (2017).
[50]N. Maleeva, L. Grünhaupt, T. Klein, F. Levy-Bertrand, O. Dupre, M. Calvo, F. Valenti, P. Winkel, F. Friedrich, W. Wernsdorfer *et al.*, Nat. Commun. **9**(1), 3889 (2018).
[51]G. Deutscher, M. Gershenson, E. Grünbaum, and Y. Imry, J. Vac. Sci. Technol. **10**, 697 (1973).
[52]T. Chui, G. Deutscher, P. Lindenfeld, and W. L. McLean, Phys. Rev. B **23**, 6172 (1981).
[53]P. Ziemann, G. Heim, and W. Buckel, Solid State Commun. **27**, 1131 (1978).
[54]M. Gurvitch, M. Washington, and H. Huggins, Appl. Phys. Lett. **42**, 472 (1983).

[55]J. M. Murduck, J. Porter, W. Dozier, R. Sandell, J. Burch, J. Bulman, C. Dang, L. Lee, H. Chan, R. Simon *et al.*, IEEE Trans. Magn. **25**, 1139 (1989).

[56]C. S. Owen and D. J. Scalapino, Phys. Rev. **164**, 538 (1967).

[57]K. Schwidtal, Phys. Rev. B **2**, 2526 (1970).

[58]E. Sarnelli, S. Pagano, B. Ruggiero, and M. Russo, IEEE Trans. Magn. **27**, 2716 (1991).

[59]A. Barone, W. J. Johnson, and R. Vaglio, J. Appl. Phys. **46**, 3628 (1975).

[60]R. Monaco, V. P. Koshelets, A. Mukhortova, and J. Mygind, Supercond. Sci. Technol. **26**, 055021 (2013).

[61]M. Weihnacht, Phys. Status Solidi B **32**, K169 (1969).

[62]R. A. Ferrell and R. E. Prange, Phys. Rev. Lett. **10**, 479 (1963).

[63]M. Cirillo, T. Doderer, S. G. Lachenmann, F. Santucci, and N. Grønbech-Jensen, Phys. Rev. B **56**, 11889 (1997).

[64]M. Cirillo, N. Grønbech-Jensen, M. R. Samuelsen, M. Salerno, and G. V. Rinati, Phys. Rev. B **58**, 12377 (1998).

[65]N. Grønbech-Jensen, M. G. Castellano, F. Chiarello, M. Cirillo, C. Cosmelli, L. V. Filippenko, R. Russo, and G. Torrioli, Phys. Rev. Lett. **93**, 107002 (2004).

[66]A. Wallraff, T. Duty, O. Lukashenko, and A. V. Ustinov, Phys. Rev. Lett. **90**, 037003 (2003).

[67]J. A. Blackburn, M. Cirillo, and N. Grønbech-Jensen, Phys. Lett. A **374**, 2827 (2010).

[68]J. M. Martinis, M. H. Devoret, and J. Clarke, Phys. Rev. Lett. **55**, 1543 (1985).

[69]A. J. Dahm, A. Denenstein, T. F. Finnegan, D. N. Langenberg, and D. J. Scalapino, Phys. Rev. Lett. **20**, 859 (1968).

[70]A. Wallraff, A. Lukashenko, J. Lisenfeld, A. Kemp, M. Fistul, Y. Koval, and A. Ustinov, Nature **425**, 155 (2003).